RSC Advances

PAPER

View Article Online
View Journal | View Issue

Cite this: *RSC Adv.*, 2022, **12**, 1950

Preparation and application of polyethyleneimine-modified corncob magnetic gel for removal of Pb(II) and Cu(II) ions from aqueous solution

Zhi Chen, * Jun Zeng, Zhi-Bo Zhang, Zhi-Jie Zhang, Shan Ma, Cong-Ming Tang and Jun-Qiang Xu

As a biomass resource, corncob is a kind of agricultural by-product with wide sources and low cost. Because its composition contains a large number of functional polymers such as cellulose, chitosan, and semi chitosan, corncob can be chemically modified to prepare a variety of adsorption materials. In this study, a magnetic gel material (PEI-CC@Fe_3O_4) consisting of corncob modified by glutaraldehyde-crosslinked polyethyleneimine (PEI) was successfully prepared and applied to the adsorption of heavy metal ions in aqueous solutions. The structure, thermal stability, and adsorption of heavy metal ions of the magnetic gel material (PEI-CC@Fe_3O_4) were characterized by Fourier-transform infrared spectroscopy (FT-IR), X-ray diffraction phase analysis (XRD), scanning electron microscopy (SEM), thermogravimetric analysis (TGA), and X-ray photoelectron spectroscopy (XPS). The results showed that PEI was crosslinked to the corncob through Aldol reaction and Schiff-base reaction. The heavy metal ion adsorption experiment showed that the PEI-CC@Fe_3O_4 had better adsorption toward divalent copper ions and divalent lead ions at 303 K, and the maximum adsorption capacities reached 459.4 mg g^{-1} and 290.8 mg g^{-1}, respectively. Moreover, the study of isothermal adsorption and adsorption kinetics shows that the adsorption process is pseudo-second-order kinetics model adsorption, which belongs to Langmuir isothermal adsorption. Such excellent adsorption performance will contribute to the application of corncob biomass materials in industrial polluted wastewater.

Received 29th November 2021
Accepted 30th December 2021

DOI: 10.1039/d1ra08699e

rsc.li/rsc-advances

1. Introduction

The development of industry has led to the accumulation of heavy metals in sewage.[1–3] Heavy metals can cause serious disease if they accumulate in the human body because they are not biodegradable.[4–6] To solve this problem, researchers have developed numerous methods to eliminate heavy metal ions.[7] These technologies consist of precipitation, adsorption, ion exchange, and so on.[8–10] The adsorption method,[11] with its practicability, convenience, and environmental friendliness, has become the most frequently employed.[12] Of the large amount of agricultural waste generated each year, only a small amount is used for resource recycling, and a larger part is incinerated.[13] This not only burdens the environment but also leads to the wastage of many available resources. Corncob is one of the most common agricultural wastes. It's mainly constituted of cellulose, hemicellulose, and lignin. These macromolecules have chemical functional groups[14] (for example, hydroxyl, carboxyl, and amino) that have a certain binding capacity with metal ions; therefore, corncob is considered an excellent natural adsorbent material.[15] However, owing to the poor adsorption performance of untreated corncob, it needs to be chemically or physically modified to improve its adsorption performance.[16] For example, biomass-activated carbon,[17] acid–base reagents,[18,19] esterification,[20] and polymer grafting[21] have been used to modify corncobs. The following exhibit that corncob-based adsorbents have a particular talent to transfer most heavy metal ions.[22] The elimination result of the modified corncob is best than that of the unmodified corncob.[23,24] However, the cell wall structure of biomass greatly reduces the adsorption effect of the constituent functional groups toward heavy metal ions. Thus, it is imperative to exploit a fresh approach to form a corncob base and enhance the adsorption performance of the adsorbent material.

Polyethyleneimine (PEI) is consists of a huge figure of free amino groups. Therefore, it can combine with heavy metal ions through electrostatic action or coordination complexation,[25–27] thus showing strong adsorption performance. However, PEI cannot be employed as an adsorbent alone because of its perfect water solubility. Thus reducing its direct use as an adsorbent for water treatment.[28–30]

Therefore, in this study, the glutaraldehyde cross-linker methodology was accustomed to graft PEI onto alkali-pretreated corncobs, and magnetic particles were added to prepare PEI-modified corncob magnetic gel adsorption

College of Chemistry and Chemical Engineering, Chongqing University of Technology, Chongqing 400054, P. R. China

materials. The adsorption performance and influencing factors of divalent copper ion and divalent lead ion were studied, and the related adsorption mechanism was investigated. This study has certain theoretical and sensible significance for the analysis, development, and adhibition of adsorption materials based on biomass as raw materials.

2. Experimental

2.1 Materials and reagents

The soft and white part of the corncob sponge layer in the middle of the corncob was crushed into the 60-mesh size and dried for later use as the raw material, defined as CC. Polyethyleneimine and sodium sulfite (≥98%, A.R. grade) were purchased from Shanghai Titan Technology Co., Ltd, Shanghai, China. Glutaraldehyde (A.R. grade, ≥50% solution), lead nitrate (A.R. grade, ≥98%), iron(III) chloride hexahydrate (A.R. grade, ≥97%), and copper nitrate (A.R. grade, ≥98%) were purchased from Chengdu Kelon Chemical Reagent Factory, Chengdu, China. All other reagents were purchased as an analytical grade, and all solutions were prepared with deionized water (the electrical resistivity was 18.2 MΩ cm at 25 °C, GWB1T/2T water purification system from Beijing Puxi General Instrument Co., Ltd, Beijing, China).

2.2 Preparation of modified corncob gel

Polyethyleneimine was grafted onto corncob by crosslinking with glutaraldehyde.[31] The specific experimental steps are as follows: the corncob was placed into a three-mouth flask containing an appropriate amount of NaOH solution and then sonicated for 30 min. Afterward, the system was stirred for 4 h under nitrogen at 25 °C, and a certain amount of PEI solutions was added dropwise, after which the system was stirred again for 40 min. Finally, an appropriate amount of glutaraldehyde was added for crosslinking. The obtained product, modified corncob gel was washed with water to neutrality, freeze-vacuum-dried (temperature: <−50 °C, vacuum pressure <5 Pa), and pulverized to obtain the PEI-modified corncob gel material, denoted as PEI-CC.

2.3 Preparation of modified corncob magnetic gel

Magnetic particles of Fe_3O_4 were embedded in the gel material through the coprecipitation method.[32] First, a solution with Fe^{3+} was prepared (1.207 g $FeCl_3 \cdot 6H_2O$ is placed in a three-necked flask containing 90 mL deionized water). And 0.094 g of anhydrous sodium sulfite was added. Then, add PEI-CC while shaking the mixture under a nitrogen environment for 2 h. After the mixture was heated to 333 K, ammonia was added drop-wise and continuously stirred for one hour. Wash the prepared modified corncob magnetic gel with deionized water to neutrality, and finally, a brown solid powder material was obtained by freeze-vacuum drying, named PEI-CC@Fe_3O_4. The preparation process and application effect are illustrated in Fig. 1.

2.4 Material characterization

The surface of the sample was gold-sprayed, and the morphology of the PEI-CC@Fe_3O_4 gel material was observed using scanning electron microscopy (SEM, Zeiss EVO18, Germany). The Fourier-transform infrared spectroscopy (FT-IR, Nicolet iS 50, USA) was exploited to detect the surface groups of gel materials. The thermal stability analysis was conducted using a thermogravimetric analyzer (TGA, Netzsch STA2500, Germany). The crystal structure was characterized *via* X-ray diffraction phase analysis (XRD, Shimadzu, XRD-7000, JPN). X-ray photoelectron spectroscopy (XPS, Thermo Fisher Scientific K-Alpha, USA) was employed for an XPS energy spectrum test (and the energy standard of charge correction is C 1s = 284.80 eV).

2.5 Adsorption experiment

An experiment was done through a batch processing method. Copper nitrate and lead nitrate were added to deionized water to produce divalent copper ion and divalent lead ion stock solution (1000 mg L^{-1}), respectively. The solution was configured to specific concentrations as required.

Divalent copper ion and divalent lead ion solutions were placed in 20 mL glass bottles, and the solution pH was adjusted using HCl solution. An amount of PEI-CC@Fe_3O_4 gel material was joined to the solution. After adsorption in a constant-temperature, shaking box for a certain period, the residual concentration of heavy metal ions was governed by atomic absorption spectrometry. Thus, the adsorption capacity is calculated. The removal rate and the adsorption amount were counted using eqn (1) and (2):

$$\eta = \frac{C_0 - C_e}{C_0} \times 100\%, \quad (1)$$

$$Q_e = \frac{C_0 - C_e}{m} \times V, \quad (2)$$

where: η is the removal rate, %; C_0 and C_e are respectively the mass concentrations before and after adsorption, mg L^{-1}; Q_e is the adsorption capacity, mg g^{-1}; V is the volume of solution, L; m is the dosage of material, g.

The effect of adsorption time on the divalent copper ion and divalent lead ion removal was determined through batch experiments. Different concentrations of adsorbent (0.3, 0.5, 1, 1.5, 2, 3, 4, 5 g L^{-1}) were added at 303 K, which is to examine the force of concentration on the adsorption of divalent copper ion and divalent lead ion. To research the effect of initial concentrations of divalent copper ion and divalent lead ion, the experiment was carried out with different preliminary concentrations (100–1000 mg L^{-1}). In the experiment, the pH value was adjusted from 1 to 5 to explore the impact of solution pH on adsorption. The influence of adsorption temperature on adsorption was examined by adjusting the temperature (293 K, 303 K, 313 K, 323 K, 333 K).

3. Results and discussion

3.1 Material characterizations

3.1.1 FT-IR. FT-IR is a means that can be used to detect the surface groups of adsorbent materials. The FT-IR spectra of corncobs (CC) and PEI-modified corncobs (PEI-CC@Fe_3O_4) are shown in Fig. 2a. The change caused by the stretching vibration of the O–H group can be seen at 3404 cm^{-1}.[33] The appearance of

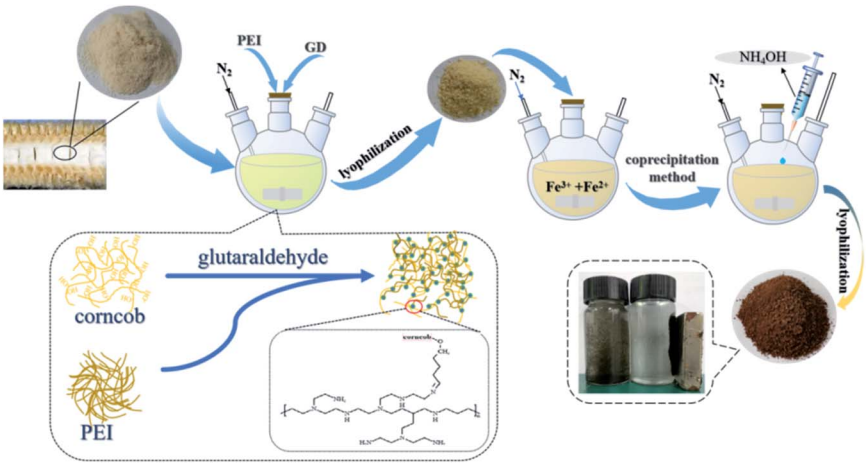

Fig. 1 Preparation and application of PEI-CC@Fe_3O_4.

the adsorption band at 2934–2834 cm^{-1} is due to C–H stretching, while the characteristic of carbon radicals extending from –COOH is located near 1730 and 1634 cm^{-1}.[34] The peak displayed in the range of 1300–1000 cm^{-1} is the characteristic absorption peak of C–O.[14,19] The peak at 899 cm^{-1} is the characteristic absorption peak of β-D-glycosidic bonds[35] between glucose unit.

Owing to the superposition of the –OH bond in the PEI-modified corncob and the N–H bond stretching vibration of PEI, the peak of the PEI-CC@Fe_3O_4 spectrum at 3389 cm^{-1} was wider and stronger than the corresponding peak of the CC spectrum. Moreover, due to the stretching vibration of the C–N bond, a new peak of 1464 cm^{-1} appears in the PEI-CC@Fe_3O_4 spectrum.[36,37] The PEI-CC@Fe_3O_4 spectrum showed no peak at 1730 cm^{-1}, indicating that hemicellulose in the raw material had been degraded. The C=N tensile vibration peak is 1634 cm^{-1} and 1654 cm^{-1} in the FT-IR of CC and PEI-CC@Fe_3O_4.[38] This proves that PEI successfully modified the corncob by crosslinking with glutaraldehyde.

In general, the oxygen-containing functional groups (carboxyl and hydroxyl) and the introduced amino groups on the corncob are involved in the binding of heavy metal ions, which indicates that the surface complexation may be the adsorption mechanism of the corncob for heavy metal ions.

3.1.2 Material TG analysis. The TG analysis results of CC and PEI-CC@Fe_3O_4 are presented in Fig. 2b. For PEI-CC@Fe_3O_4, three thermal decomposition stages occurred. The first-stage degradation (below 473 K, about 4 wt% loss) was caused by the loss of moisture in the materials, which points out the PEI-CC@Fe_3O_4 had hydrophilic owing to the existence of PEI. The

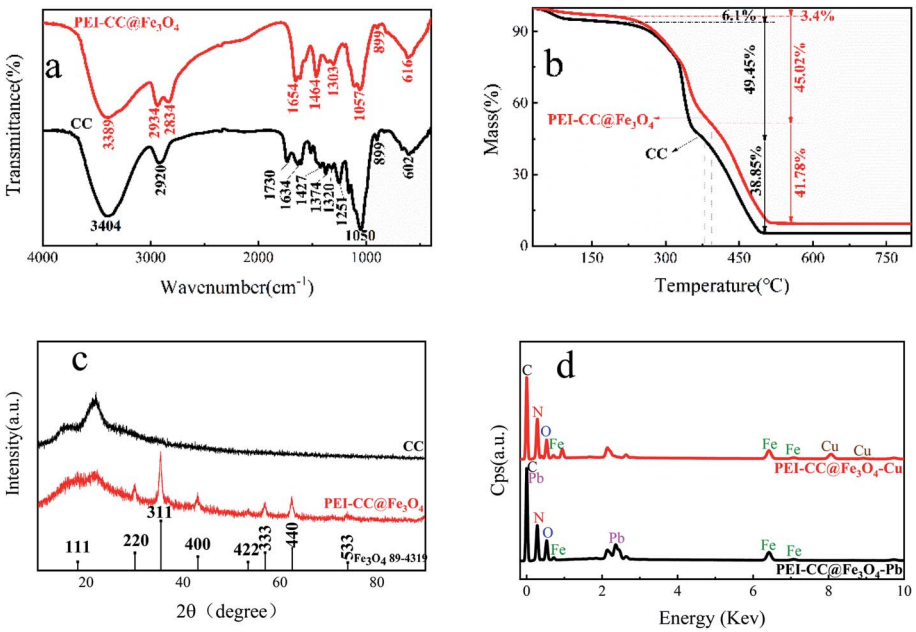

Fig. 2 FTIR (a), TG (b), XRD (c), and EDS (d) of CC and PEI-CC@Fe_3O_4.

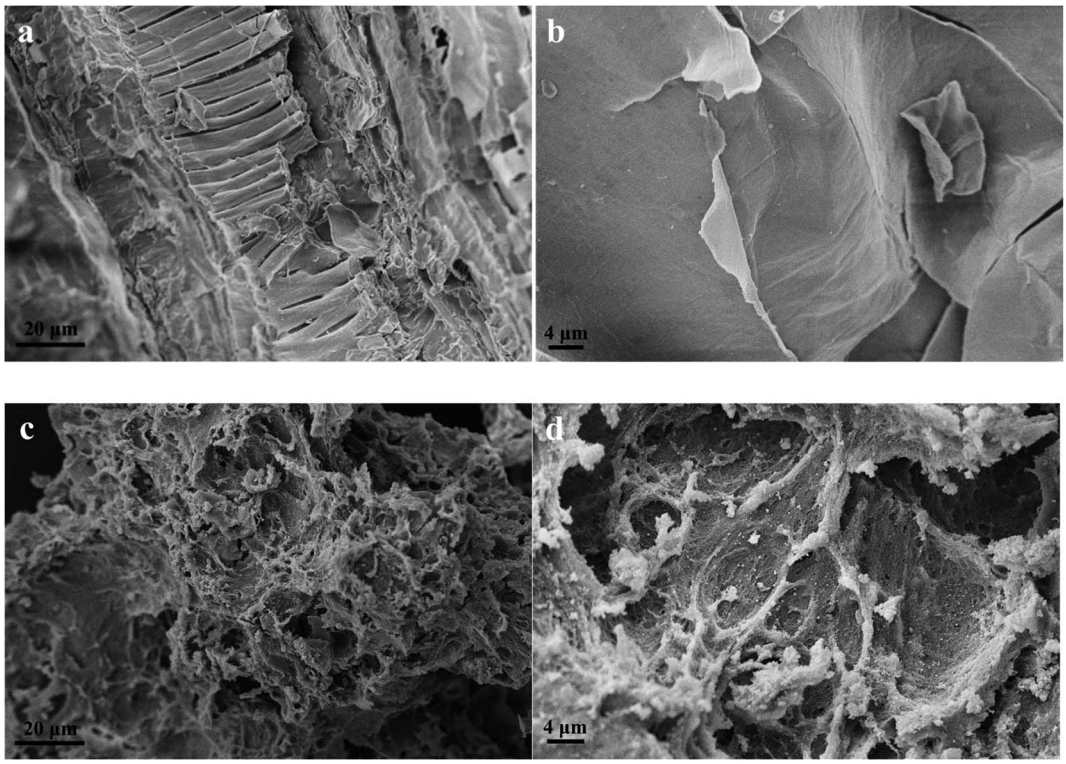

Fig. 3 Scanning electron microscopy image of CC: (a) 2000× and (b) 5000×; scanning electron microscopy image of PEI-CC@Fe_3O_4: (c) 2000× and (d) 5000×.

second-stage decomposition (between 473 K and 653 K, about 42 wt% loss) was linked to the degradation of the polymer. The third-stage decomposition (between 653 K and 823 K, about 45 wt% loss) was revealed to the carbonization of the heterogeneous polymer shell and the occurrence of amorphous iron oxide. The excess accounted for about 9 wt% and included carbonized polymer materials and magnetic Fe_3O_4 nanoparticles. The decomposition temperature of PEI-CC@Fe_3O_4 was different from that of CC because of the structural change caused by chemical modification. This indicates that the thermal stability of corncob material was developed by PEI modification. The crosslinking reaction between PEI, glutaraldehyde, and corncob (condensation reaction and the generation of Schiff base) improved the material thermal stability.

3.1.3 XRD analysis. The XRD pattern of PEI-CC@Fe_3O_4 (Fig. 2c) has eight characteristic peaks, at $2\theta = 18.3°$, 30.1°, 35.4°, 43.1°, 53.4°, 56.9°, 62.5°, and 74.0°; these peaks correspond to the (111), (220), (311), (400), (422), (333), (440), and (622) planes of magnetic Fe_3O_4 with a spinel structure, individually. The surface diffraction peaks agree with the standard card (Fe_3O_4 89-4319). This indicates that the crystal structure of the PEI-modified corncob with glutaraldehyde crosslinked branches was the same as that of the unmodified corncob and that Fe_3O_4 magnetic particles were successfully added to the gel. As shown in Fig. 2, the spectra of the unmodified and modified corncobs had peaked at 22° and 17°, respectively. The two peaks are the (002) crystal plane diffraction peak (crystalline area) and (101) plane diffraction peak (amorphous area) of cellulose, respectively. Furthermore, the relative intensities of the diffraction peaks at 22° and 17° changed after NaOH solution and ultrasonic treatment; this indicates that the treatment method had an impact on both the crystalline and amorphous regions of the corncob cellulose, and the impact on the crystalline region was more significant. The possible reason for this phenomenon is that under ultrasonic alkaline conditions, the alkaline solution can destroy the crystalline structure of the crystalline area through swelling, and the hemicellulose and lignin in the amorphous region can be removed.

3.1.4 SEM-EDS analysis. Fig. 3a shows the SEM image of the untreated corncob at 2000× magnification, and Fig. 3b is a partially enlarged view of Fig. 3a. As shown in the figure, the corncob presented a smooth surface and tightly connected strip structure. Fig. 3c shows the SEM image of the PEI-modified corncob at 2000× magnification, and Fig. 3d is the partially enlarged view of Fig. 3c. As shown in the SEM images, the internal structure of the corncob underwent tremendous changes after PEI modification. The dense striped structure became a loose and porous network structure, which significantly increased the specific surface area of the corncob. The porous three-dimensional network structure facilitates the penetration of the solution into the material, and it provides a convenient area for adsorption. The EDS spectrum of the modified corncob featured characteristic peaks of C, N, O, Fe, and Cu/Pb in Fig. 2d. This further confirms that the magnetic particles (Fe_3O_4) were successfully embedded in the gel and that divalent copper ion and divalent lead ion were successfully adsorbed by PEI-CC@Fe_3O_4. However, since the divalent copper

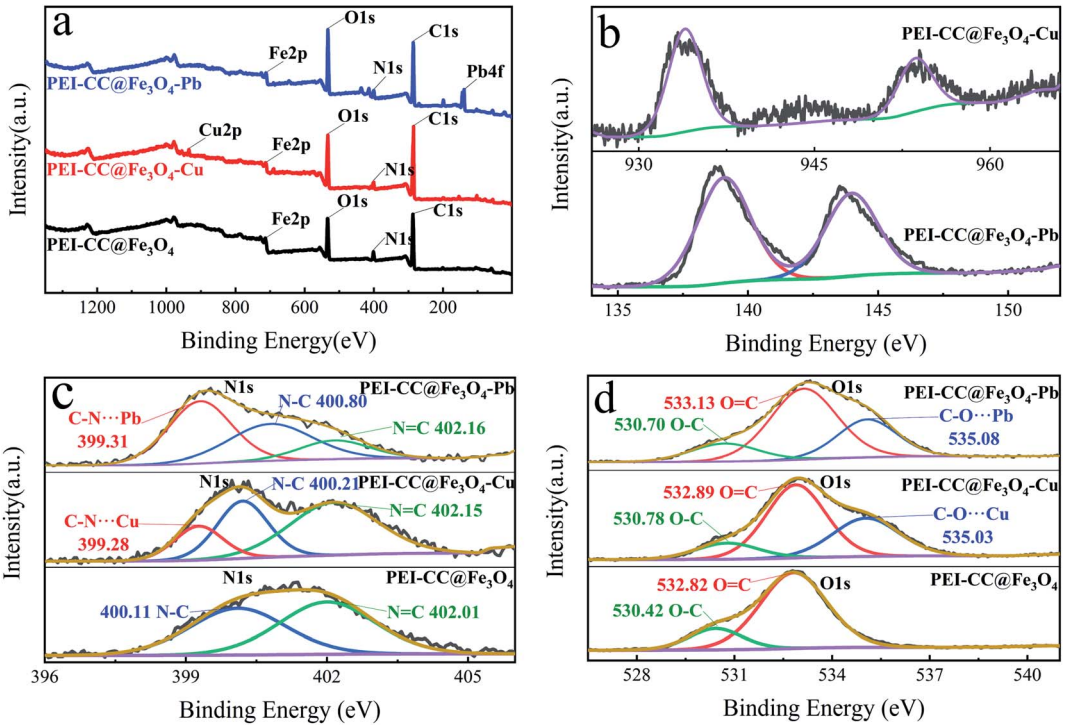

Fig. 4 XPS of PEI-CC@Fe_3O_4 before and after adsorption: (a) full spectrum; (b) PEI-CC@Fe_3O_4–Pb, PEI-CC@Fe_3O_4–Cu; (c) N 1s; (d) O 1s.

ion and divalent lead ion contents were lower than the C, N, and O contents, the peak value was not high.

3.1.5 XPS. To better explain the adsorption mechanism of PEI-CC@Fe_3O_4 toward divalent copper ion and divalent lead ion. XPS was used to examine chemical information and the type of divalent copper ion and divalent lead ion on the PEI-modified corncob before and after adsorption (Fig. 4). Fe 2p characteristic peaks appeared in the spectrum of the corncob after adsorption (Fig. 4a). It indicates that the magnetic particles were successfully embedded in the modified corncob material. Fig. 4b shows the characteristic peaks of divalent copper ion and divalent lead ion, indicating that divalent copper ion and divalent lead ion were successfully adsorbed. From previous reports, functional groups may be the factors affecting the clearance of heavy metal by modified biomass. The adsorption mechanism of heavy metal ions on modified biomass includes coordination complexation, ion exchange, and chelation.[39–41] The O 1s spectra of divalent copper ion and divalent lead ion adsorbed by PEI-CC@Fe_3O_4 are shown in Fig. 4c. After adsorption, the peaks of O–C and O=C[42,43] shifted to higher binding energies, and new peaks occurred at 535.03 eV and 535.08 eV. The increase in binding energy after the adsorption of divalent copper ion and divalent lead ion occurred because oxygen atoms shared electrons with Cu and Pb, which lessened the electron density of nitrogen atoms and increased the binding energy. The binding energies peaks of 535.03 eV and 535.08 eV can be blamed on the coordination forms of C–O···Cu and C–O···Pb.[44,45] Similarly, in the N 1s narrow-spectrum before adsorption (Fig. 4d), the characteristic peaks at 400.12 eV and 402.01 eV relate to N–C and N=C, individually, and the binding energies of the two characteristic peaks increased after adsorption. This was because nitrogen atoms shared electrons with Cu and Pb, which lessened nitrogen atom electron cloud density and increased their binding energy. New peaks occurred at 399.28 eV and 399.31 eV, because of the existence of C–NH···Pb and C–NH···Cu.[46,47] During the adsorption course of divalent copper ion and divalent lead ion, strong coordination and complexation occurred between the material and $–NH_2$ and –OH; thus, the introduction of $–NH_2$ in PEI improved the adsorption effect of heavy metals.

3.2 Divalent copper ion and divalent lead ion adsorption experiment

3.2.1 Impact of adsorption time. Fig. 5a indications the clout of adsorption time for adsorption degree of divalent copper ion and divalent lead ion at 303 K, pH 5, the material concentration of 1 g L^{-1}, and initial concentrations of divalent copper ion and divalent lead ion of 500 mg L^{-1}. As noted in the figure, the adsorption reaction continued to change with the contact time of PEI-CC@Fe_3O_4 with divalent copper ion and divalent lead ion until divalent copper ion and divalent lead ion reached adsorption equilibrium. The adsorption process of PEI-CC@Fe_3O_4 toward divalent copper ion and divalent lead ion can be divided into two stages: fast (60 min) and slow (60–120 min). After 120 min, the adsorption gradually reached equilibrium. This trend occurred because as the adsorption reaction continued, the concentration gradient of divalent copper ion and divalent lead ion on the PEI-CC@Fe_3O_4 surface in the solution became increasingly smaller, which reduced the driving force behind adsorption, thereby reducing the

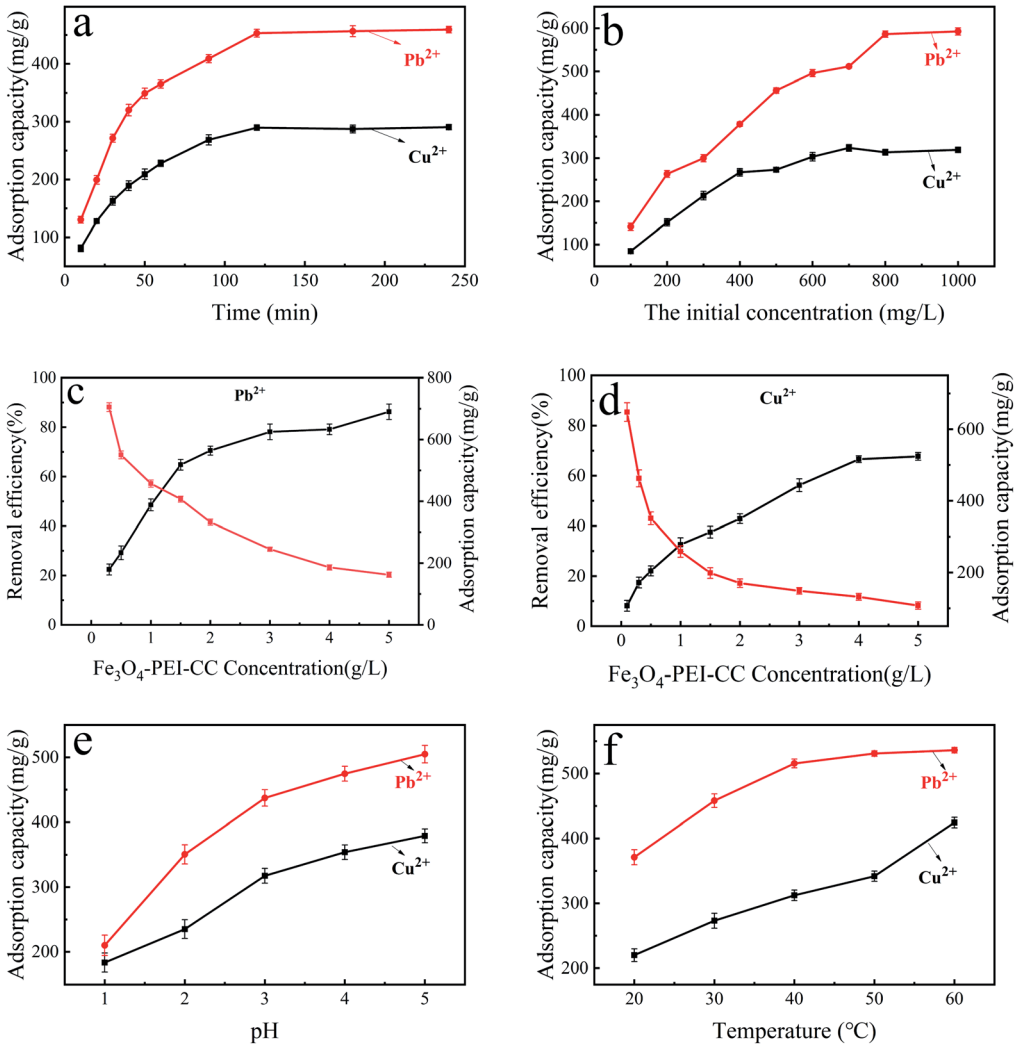

Fig. 5 (a) PEI-CC@Fe_3O_4 adsorption of heavy metals is affected by adsorption time. (b) Effect of initial solution concentration on PEI-CC@Fe_3O_4 adsorption of heavy metals. (c and d) PEI-CC@Fe_3O_4 effect of dose on adsorption. (e) Adsorption capacity of PEI-CC@Fe_3O_4 for heavy metals at different initial solution pH. (f) Temperature on the adsorptions of divalent copper ion and divalent lead ion.

adsorption efficiency. In addition, the adsorption sites on the PEI-CC@Fe_3O_4 surface were gradually occupied, resulting in increasingly fewer active sites available for adsorption, which also reduced the adsorption rate. Furthermore, the divalent copper ion and divalent lead ion adsorbed on the PEI-CC@Fe_3O_4 surface would repel the remaining divalent copper ion and divalent lead ion in solution and hinder further adsorption of them. Therefore, the adsorption capacity gradually tended to balance.

3.2.2 Effect of the initial concentration of the solution. It is given that the effect of the initial concentration of the solution on the adsorption effects of divalent copper ion and divalent lead ion at 303 K, 4 h, pH 5, and material concentration is 1 g L^{-1} in Fig. 5b. When the initial divalent metal ion concentration increased to 1000 mg L^{-1}, the adsorption capacity of PEI-CC@Fe_3O_4 toward divalent lead ion increased to 592.8 mg g^{-1}, and the adsorption capacity toward divalent copper ion continuously increased to 319.2 mg g^{-1}. Because of increasing the initial divalent metal ion concentration, the concentration gradient of divalent copper ion and lead ion on the surface of the solution and PEI-CC@Fe_3O_4 increased, increasing the mass transfer rate and the equilibrium adsorption capacity.

3.2.3 Influence of PEI-CC@Fe_3O_4 dosage. Fig. 5c and d show the effect of the PEI-CC@Fe_3O_4 dosage of the solution on the adsorption rate of divalent copper ion and divalent lead ion at 303 K, 4 h, pH 5, and initial concentrations of divalent copper ion and divalent lead ion of 500 mg L^{-1}. With the increase in the PEI-CC@Fe_3O_4 concentration to 5 g L^{-1}, the removal rate of divalent lead ion raised to 67.75%, but the adsorption amount diminished to 107.688 mg g^{-1}, and the divalent lead ion removal rate increased to 86.3%, but the adsorption amount decreased 162.628 mg g^{-1}. This phenomenon shows that when the concentration of divalent copper ion and divalent lead ion is constant, increasing the PEI-CC@Fe_3O_4 concentration will increase the active sites available for adsorption. PEI-CC@Fe_3O_4 can adsorb more divalent copper

ion and divalent lead ion. With a further increase in the PEI-CC@Fe_3O_4 concentration, the increasing trend of the divalent lead ion removal rate slowed down and finally reached equilibrium, but the adsorption capacity curve still showed a downward trend. This behavior occurred because when the adsorption reached equilibrium, further increases in the PEI-CC@Fe_3O_4 concentration increased the adsorption sites, causing more adsorption materials to be unable to be fully utilized, occasioning a gradual decline in the relative adsorption power per unit of adsorption material.

3.2.4 Influence of solution pH. pH value is a crucial factor affecting adsorption. Because it affects the presence of heavy metal, surface charges, and functional groups on the material. The main forms of lead ion in solution are Pb^{2+}, $[Pb(OH)]^+$, $Pb(OH)_2$, $[Pb(OH)_3]^-$, and $[Pb(OH)_4]^{2-}$. The distribution of these forms is affected by pH. At pH ≤ 5, only Pb^{2+} exists; at pH > 5, the divalent lead ion will be hydrolyzed to produce $[Pb(OH)]^+$, $[Pb_3(OH)_4]^{2+}$, and $Pb(OH)_2$. For divalent copper ion, at pH > 5, the divalent copper ion will begin to precipitate, and when the pH reaches 6, much divalent copper ion will have already precipitated; therefore, the experiment only studied simulated wastewater containing divalent copper ion and divalent lead ion with a primary pH ≤ 5. Fig. 5e illustrates the result of pH on the sorption result of divalent copper ion and divalent lead ion at 303 K, 4 h, the material concentration of 1 g L^{-1}, and initial concentrations of divalent copper ion and divalent lead ion of 500 mg L^{-1}.

Increasing the solution's pH, the adsorption ability of PEI-CC@Fe_3O_4 toward divalent lead ion increased to 505 mg g^{-1}, while the adsorption capability of PEI-CC@Fe_3O_4 toward divalent copper ion swelled to 379.2 mg g^{-1}. The reason is the competitive adsorption of high concentration H^+ and heavy metal ions will occur at a lower pH. Therefore, H^+ occupies the active site on the PEI-CC@Fe_3O_4 surface, and adsorption of H^+ on heavy metal ions would generate electrostatic repulsion, thereby hindering the adsorption. Second, the amino and

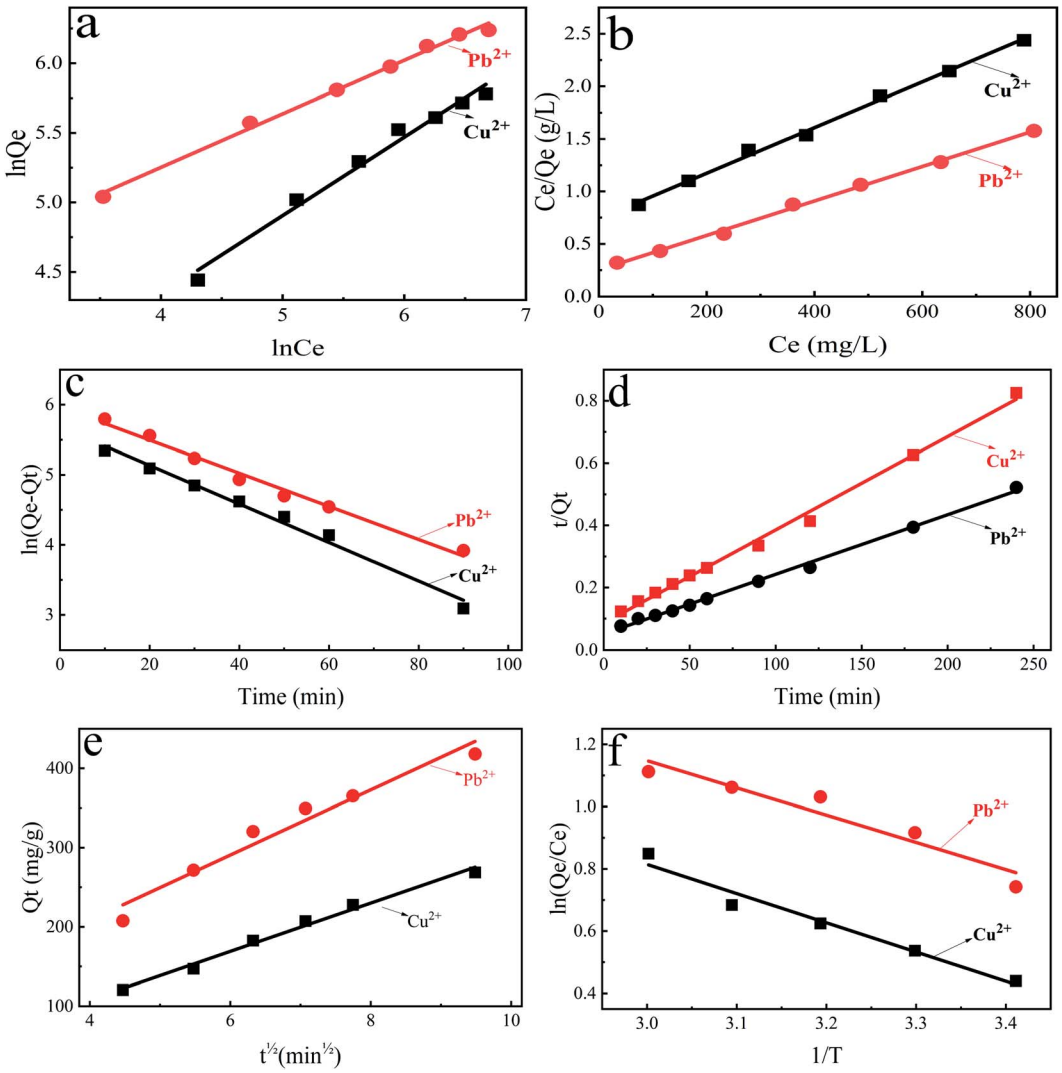

Fig. 6 Adsorption isotherms of divalent copper ion and divalent lead ion on PEI-CC@Fe_3O_4 fitted by Freundlich (a) and Langmuir (b) models. Kinetics of divalent copper ion and divalent lead ion adsorption by PEI-CC@Fe_3O_4, fitted by pseudo-first-order (c) and pseudo-second-order (d) models. Internal diffusion fitting (e). Adsorption thermodynamics (f) of PEI-CC@Fe_3O_4 toward divalent copper ion and divalent lead ion.

hydroxyl groups on the PEI-CC@Fe_3O_4 surface were highly protonated at lower pH, which also affects the ability of the groups in PEI-CC@Fe_3O_4 to coordinate with heavy metal ions. Increasing the pH, H^+ concentration goes down, protonation of amino groups and hydroxyl groups weakened, the electrostatic repulsion decreased, and the adsorption resistance of heavy metal ions dwindled, thereby raising the adsorption capacity.

3.2.5 The influence of adsorption temperature. Fig. 5f exposes the validity of the adsorption temperature on adsorption rate at pH 5, 4 h, the material concentration is 1 g L^{-1}, and preliminary concentration of divalent copper ion and divalent lead ion of 500 mg L^{-1}. With temperature change, the adsorption competence of PEI-CC@Fe_3O_4 on divalent copper ion and divalent lead ion increased. This reveals that heating up increased the contact and reaction speed of divalent copper ion and divalent lead ion with the material. Which was beneficial to adsorption, but the increased rate of the adsorption competence declined with the continuous boost in temperature. The adsorption progress of PEI-CC@Fe_3O_4 toward divalent lead ion conformed to this law. The adsorption toward divalent copper ion also conformed to the trend up to 323 K, after which the adsorption capacity suddenly increased with a further temperature increase of upto 333 K. This occurred because the very high temperature increased the ion-diffusion rate in the solution so that divalent copper ion could overcome the resistance of PEI-CC@Fe_3O_4 and enter the internal pores; thus, owing to the high temperature, the adsorption activation energy was overcome, and the adsorption capacity was increased.

3.3 Adsorption isotherm

Adsorption isotherm of metal ions is usually described by the Langmuir equation (eqn (3)) and Freundlich equation (eqn (4)), given by

$$\frac{C_e}{Q_e} = \frac{C_e}{Q_m} + \frac{1}{Q_m K_L}, \quad (3)$$

$$\ln Q_e = \frac{1}{n}\ln C_e + \ln K_F, \quad (4)$$

$$R_L = \frac{1}{1 + K_L \cdot C_{0m}}, \quad (5)$$

where: Q_e is equilibrium adsorption capacity (mg g^{-1}); C_e is equilibrium concentration (mg L^{-1}); Q_m is the maximum capacity of monolayer adsorption (mg g^{-1}); K_F and n are Freundlich adsorption equilibrium constants; R_L is separation factor; K_L is Langmuir adsorption equilibrium constant; C_{0m} represents the maximum initial concentration of the fitting process (mg g^{-1}).

The adsorption isotherm models of Langmuir and Freundlich were used to fit the adsorption data of divalent copper ion and divalent lead ion isotherms (Fig. 6a and b). The fitted data are presented in Table 1.

As shown in Table 1, R^2 of both models is greater than 0.99, but Langmuir isothermal adsorption model fits the data better than Freundlich isothermal adsorption model. Therefore, the adsorption process of divalent copper ion and divalent lead ion by PEI-CC@Fe_3O_4 be able to better described by the Langmuir equation. The premise of the Langmuir isothermal adsorption model is that the monolayer adsorption takes place on the material surface, while chemical adsorption occurs in monolayer adsorption. Therefore, the mechanism of PEI-CC@Fe_3O_4 adsorption toward divalent copper ion and divalent lead ion was mainly chemical adsorption.

In the adsorption course, R_L can settle the degree of interaction between adsorbed material and metal ions. $R_L > 1$ indicates that the adsorption is disadvantageous; when $R_L = 1$, the amount of adsorption material is linearly correlated to the adsorption capacity of metal ions. When $0 < R_L < 1$, adsorption of metal ions is favorable. When R_L is equal to 0, the adsorption procedure of the adsorbent on metal ions is irreversible when $0 < R_L < 1$, adsorption of metal ions is favorable; when $R_L = 0$, the adsorption process of metal ions is irreversible. R_L can be computed from eqn (5).

Calculated R_L values of adsorbed divalent copper ion and divalent lead ion are between 0 and 1 (0.33 and 0.18, respectively). This shows that the PEI-modified corncob magnetic gel adsorption material is beneficial to the adsorption of divalent copper ion and divalent lead ion. Moreover, the R_L value corresponding to the adsorption of divalent lead ion was less than that of divalent copper ion; thus, the measure of divalent lead ion adsorbed by PEI-CC@Fe_3O_4 was greater than divalent copper ion, which also agrees with experimental facts.

3.4 Adsorption kinetics

The experimental results of PEI-CC@Fe_3O_4 adsorption toward divalent copper ion and divalent lead ion over time are fitted by the pseudo-first-order kinetic equation (eqn (6)) and pseudo-second-order kinetic equation (eqn (7)).

$$\ln(Q_{e,exp} - Q_t) = \ln Q_{e,cal} - k_1 t, \quad (6)$$

$$\frac{t}{Q_t} = \frac{1}{k_2 \cdot Q_{e,cal}^2} + \frac{t}{Q_{e,cal}}, \quad (7)$$

Table 1 Freundlich and Langmuir constants

	Freundlich			Langmuir		
Metal ion	K_F ($mg^{1-1/n}$ $L^{1/n}$ g^{-1})	n	R^2	Q_m (mg g^{-1})	K_L (L mg^{-1})	R^2
Cu^{2+}	8.036	1.77	0.9849	460.83	2.94×10^{-3}	0.9965
Pb^{2+}	41	2.6	0.9945	609.76	6.51×10^{-3}	0.9977

Table 2 Kinetic parameters

	Pseudo-first-order kinetic model				Pseudo-second-order kinetic model		
Metal ion	$Q_{e,exp}$ (mg g^{-1})	$Q_{e,cal}$ (mg g^{-1})	K_1 (min^{-1})	R^2	$Q_{e,cal}$ (mg g^{-1})	K_2 (g mg^{-1} min^{-1})	R^2
Cu^{2+}	290.8	294.23	0.0275	0.988	333.33	1.05×10^{-4}	0.995
Pb^{2+}	459.4	391.20	0.0237	0.988	520.83	7.22×10^{-5}	0.997

Table 3 Internal diffusion parameters

	Internal diffusion		
	k_p	C (mg g^{-1})	R^2
Cu^{2+}	26.98	10.23	0.98
Pb^{2+}	40.81	33.33	0.95

$$Q_t = k_p \cdot t^{1/2} + C, \quad (8)$$

where: Q_t is the adsorption capacity of reaction time (t), mg g^{-1}; $Q_{e,exp}$ and $Q_{e,cal}$ is the equilibrium adsorption capacities obtained by experiment and simulation, respectively, mg g^{-1}; k_1 is the quasi-first-order rate constant, min^{-1}; k_2 is the quasi-second-order rate constant, g (mg min)$^{-1}$; t is the adsorption time, min; k_p is the internal diffusion rate constant, and C is a constant.

The pseudo-second-order kinetic model can well-mannered communicate the adsorption of divalent copper ion and divalent lead ion by PEI-CC@Fe_3O_4 ($R^2 > 0.99$). The specific data is in Table 2. The saturated adsorption capacity calculated by the pseudo-second-order kinetics model is more conform to the actual situation. It is indicated PEI-CC@Fe_3O_4 mainly adsorbed divalent copper ion and divalent lead ion through chemical adsorption.

The adsorption reaction process is generally divided into three steps: external diffusion, internal diffusion, and chemical adsorption. External diffusion is mainly caused by the rapid and full shaking of the solution, while in internal diffusion, the solute diffuses into the inside through the pores of material, and the internal diffusion will be accompanied by the progress of chemical adsorption. Usually, the adsorption rate-control step is determined by the latter two steps. By fitting the experimental data (Fig. 6e), we can determine the key rate-controlling steps. The fitting formula is shown in eqn (8).

The larger the K_p value, the easier it is for the adsorbate to diffuse inside the adsorbent. If the origin is on a line describing the relationship between Q_t and $t^{1/2}$, then internal diffusion is a rate-controlled process.

As presented in Table 3, the internal diffusion rate constant k_p of divalent copper ion is smaller than divalent lead ion, indicating that divalent lead ion diffused more easily in the adsorbent material than divalent copper ion. The fitting line does not cross the origin, indicating that the rate control process is not internal diffusion. Therefore, the adsorption of divalent copper ion and divalent lead ion by PEI-CC@Fe_3O_4 was mainly by chemical adsorption, while internal diffusion was secondary.

3.5 Adsorption thermodynamics

The adsorption thermodynamics of PEI-CC@Fe_3O_4 gel adsorption material can be expressed by the following equations:

$$\ln\left(\frac{Q_e}{C_e}\right) = \frac{\Delta S}{R} - \frac{\Delta H}{RT}, \quad (9)$$

$$\Delta G = \Delta H - T\Delta S, \quad (10)$$

where: ΔH is enthalpy change; ΔS is denoted entropy change; ΔG is a change of Gibbs free energy; Q_e is saturated adsorption capacity (mg g^{-1}); C_e is a concentration of heavy metal ions (mg L^{-1}).

According to temperature change data, the results of PEI-CC@Fe_3O_4 adsorption toward divalent copper ion and divalent lead ion were fitted (Fig. 6f).

Adsorption thermodynamics of divalent copper ion and divalent lead ion adsorption on the PEI-CC@Fe_3O_4 were investigated at 308 K (Table 4). For the adsorption of divalent copper ion and divalent lead ion, the ΔG values at dissimilar temperatures were less than zero. This indicates that the adsorption of divalent copper ion and divalent lead ion by PEI-CC@Fe_3O_4 was spontaneous. The absolute value of ΔG increases with the increase of temperature. The results show that with the increase of temperature, the higher the driving force behind the reaction process, the easier the adsorption. This is consistent with the endothermic reaction of the adsorption process ($\Delta H > 0$) and the explanation that high temperature is beneficial to adsorption. Moreover, $\Delta S > 0$ indicates that the disorder of solid–liquid

Table 4 Thermodynamic parameters

	ΔG (kJ mol^{-1})						
T (K)	293.15	303.15	313.15	323.15	333.15	ΔS [J (mol^{-1} K^{-1})]	ΔH (kJ mol^{-1})
Cu^{2+}	−1.04	−1.35	−1.65	−1.95	−2.25	30.20	7.81
Pb^{2+}	−1.92	−2.23	−2.55	−2.86	−3.17	31.36	7.27

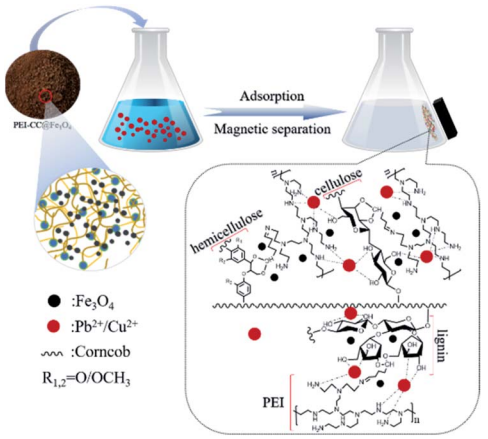

Fig. 7 Interaction mechanisms between metal ions and PEI-CC@Fe_3O_4.

level increases. Fig. 7 illustrates the interaction mechanism between metal ions and PEI-CC@Fe_3O_4.

4. Conclusion

In this study, a PEI-modified corncob magnetic gel material was prepared using agricultural waste corncob as the raw material, PEI as a modifier, glutaraldehyde as a crosslinking agent, and Fe_3O_4 as magnetic particles. Experiments showed that the PEI-CC@Fe_3O_4 has nice adsorption enactment toward divalent copper ion and divalent lead ion in wastewater and that it is a better adsorption material for wastewater containing heavy metals. Moreover, the addition of magnetic particles could improve the separation efficiency after the adsorption material adsorbs the metal ions so that the material can be recycled more conveniently and cost savings are higher.

The adsorption process of PEI-CC@Fe_3O_4 is more in line with the quasi-second-order kinetic model, indicating that chemisorption was dominant. The internal diffusion parameters were also explored, and discovering the internal diffusion rate constant k_p of divalent copper ion was smaller than that of the divalent lead ion. Indicating that divalent lead ion could more easily diffuse into the adsorbent material than divalent copper ion, and the rate-controlling stage was not internal diffusion. Therefore, the adsorption of divalent copper ion and divalent lead ion by this material is mainly by chemical adsorption, while internal diffusion is secondary.

The Langmuir and the Freundlich adsorption isotherm model were exploited to fitting the isotherms of the adsorption of divalent copper ion and divalent lead ion by the modified corncob. The Langmuir adsorption isotherm model had a better linear fit. The thermodynamic parameters show that under the research conditions, the elimination of divalent copper ion and divalent lead ion by the PEI-CC@Fe_3O_4 material was spontaneous and endothermic.

Conflicts of interest

There are no conflicts to declare.

Acknowledgements

The authors are grateful for the financial support from the Chongqing Municipal Education Commission (KJQN201801112) and the Chongqing Municipal Science & Technology Commission (cstc2019jcyj-msxmX0232).

References

1 M. E. Lee, J. H. Park and J. W. Chung, *J. Environ. Manage.*, 2019, **236**, 118–124.
2 G. K. Dutta and N. Karak, *RSC Adv.*, 2019, **9**, 20829–20840.
3 R. Foroutan, S. J. Peighambardoust, S. Hemmati, A. Ahmadi, E. Falletta, B. Ramavandi and C. L. Bianchi, *RSC Adv.*, 2021, **11**, 27309–27321.
4 J. Gao, K. Y. Wang and T.-S. Chung, *J. Membr. Sci.*, 2020, **603**, 118022.
5 Q. Liu, G.-L. Zang and Q. Zhao, *RSC Adv.*, 2021, **11**, 25880–25891.
6 P. T. Tho, H. T. Van, L. H. Nguyen, T. K. Hoang, T. N. Ha Tran, T. T. Nguyen, T. B. Hanh Nguyen, V. Q. Nguyen, H. Le Sy, V. N. Thai, Q. B. Tran, S. M. Sadeghzadeh, R. Asadpour and P. Q. Thang, *RSC Adv.*, 2021, **11**, 18881–18897.
7 J. Zhang, H. Chen, Z. Chen, J. He, W. Shi, D. Liu, H. Chi, F. Cui and W. Wang, *RSC Adv.*, 2016, **6**, 59292–59298.
8 N. F. Campos, G. A. J. C. Guedes, L. P. S. Oliveira, B. M. V. Gama, D. C. S. Sales, J. M. Rodríguez-Díaz, C. M. B. M. Barbosa and M. M. M. B. Duarte, *J. Environ. Chem. Eng.*, 2020, **8**, 104232.
9 H. Demiral and C. Güngör, *J. Cleaner Prod.*, 2016, **124**, 103–113.
10 N. A. Fakhre and B. M. Ibrahim, *J. Hazard. Mater.*, 2018, **343**, 324–331.
11 R. Baby, B. Saifullah and M. Z. Hussein, *Sci. Rep.*, 2019, **9**, 18955.
12 H. Wang, X. Lai, W. Zhao, Y. Chen, X. Yang, X. Meng and Y. Li, *RSC Adv.*, 2019, **9**, 21996–22003.
13 H. O. Chukwuemeka-Okorie, P. N. Ekemezie, K. G. Akpomie and C. S. Olikagu, *Front. Chem.*, 2018, **6**, 273.
14 N. V. Sych, S. I. Trofymenko, O. I. Poddubnaya, M. M. Tsyba, V. I. Sapsay, D. O. Klymchuk and A. M. Puziy, *Appl. Surf. Sci.*, 2012, **261**, 75–82.
15 J. Zhao, L. Yu, F. Zhou, H. Ma, K. Yang and G. Wu, *RSC Adv.*, 2021, **11**, 8025–8032.
16 S. Vafakhah, M. E. Bahrololoom, R. Bazarganlari and M. Saeedikhani, *J. Environ. Chem. Eng.*, 2014, **2**, 356–361.
17 J. K. Nduka, *Int. J. Chem. Eng.*, 2012, **2012**, 1–7.
18 R. Leyva-Ramos, L. E. Landin-Rodriguez, S. Leyva-Ramos and N. A. Medellin-Castillo, *Chem. Eng. J.*, 2012, **180**, 113–120.
19 Z. Liu, Y. Sun, X. Xu, X. Meng, J. Qu, Z. Wang, C. Liu and B. Qu, *Bioresour. Technol.*, 2020, **306**, 123154.
20 G. Tan, H. Yuan, Y. Liu and D. Xiao, *J. Hazard. Mater.*, 2010, **174**, 740–745.
21 Y. Shi, T. Zhang, H. Ren, A. Kruse and R. Cui, *Bioresour. Technol.*, 2018, **247**, 370–379.
22 A. Zheng, K. Zhao, L. Li, Z. Zhao, L. Jiang, Z. Huang, G. Wei, F. He and H. Li, *J. Energy Inst.*, 2018, **91**, 676–682.

23 S. Chen, Q. Yue, B. Gao, Q. Li and X. Xu, *Chem. Eng. J.*, 2011, **168**, 909–917.
24 J. L. Liu, W. C. Qian, J. Z. Guo, Y. Shen and B. Li, *Bioresour. Technol.*, 2021, **320**, 124374.
25 J. Tang, L. Xiang, J. Fan, Z. Cui and H. Wu, *Environ. Earth Sci.*, 2018, **77**, 441.
26 S. Tangtubtim and S. Saikrasun, *Appl. Surf. Sci.*, 2019, **467–468**, 596–607.
27 J. Wang, Q. Xie, A. Li, X. Liu, F. Yu and J. Ji, *Water Sci. Technol.*, 2020, **81**, 1114–1129.
28 B. Qiu, J. Guo, X. Zhang, D. Sun, H. Gu, Q. Wang, H. Wang, X. Wang, X. Zhang, B. L. Weeks, Z. Guo and S. Wei, *ACS Appl. Mater. Interfaces*, 2014, **6**, 19816–19824.
29 X. Wang, J. Feng, Y. Cai, M. Fang, M. Kong, A. Alsaedi, T. Hayat and X. Tan, *Sci. Total Environ.*, 2020, **708**, 134575.
30 S. Wong, H. H. Tumari, N. Ngadi, N. B. Mohamed, O. Hassan, R. Mat and N. A. Saidina Amin, *J. Cleaner Prod.*, 2019, **206**, 394–406.
31 F. Bucatariu, C. A. Ghiorghita, M. M. Zaharia, S. Schwarz, F. Simon and M. Mihai, *ACS Appl. Mater. Interfaces*, 2020, **12**, 37585–37596.
32 P. Kulal and V. Badalamoole, *Int. J. Biol. Macromol.*, 2020, **156**, 1408–1417.
33 H. Ma, J. B. Li, W. W. Liu, M. Miao, B. J. Cheng and S. W. Zhu, *Bioresour. Technol.*, 2015, **190**, 13–20.
34 C. Duan, X. Meng, C. Liu, W. Lu, J. Liu, L. Dai, W. Wang, W. Zhao, C. Xiong and Y. Ni, *Carbohydr. Polym.*, 2019, **222**, 115042.
35 R. Fonseca-Correa, L. Giraldo and J. C. Moreno-Piraján, *J. Anal. Appl. Pyrolysis*, 2013, **101**, 132–141.
36 H. Lin, S. Han, Y. Dong and Y. He, *Appl. Surf. Sci.*, 2017, **412**, 152–159.
37 Y. Xiong, X. Cui, D. Wang, Y. Wang, Z. Lou, W. Shan and Y. Fan, *Mater. Sci. Eng., C*, 2019, **99**, 1115–1122.
38 S. Sadeghi, H. R. Zakeri, M. H. Saghi, S. K. Ghadiri, S. S. Talebi, M. Shams and G. L. Dotto, *Environ. Sci. Pollut. Res.*, 2021, **28**, 3556–3565.
39 X. Huang, L. Wang, J. Zhang, X. Du, S. Wu, H. Wang and X. Wei, *Int. J. Biol. Macromol.*, 2020, **163**, 1915–1925.
40 M. Liu, L. Jia, Z. Zhao, Y. Han, Y. Li, Q. Peng and Q. Zhang, *Chem. Eng. J.*, 2020, **390**, 124667.
41 L. Qiao, S. Li, Y. Li, Y. Liu and K. Du, *J. Cleaner Prod.*, 2020, **253**, 120017.
42 A. L. Popovic, J. D. Rusmirovic, Z. Velickovic, Z. Radovanovic, M. Ristic, V. P. Pavlovic and A. D. Marinkovic, *Int. J. Biol. Macromol.*, 2020, **156**, 1160–1173.
43 Y. Yan, Y. Wang, J. Wu, Z. Wang, X. Shen, Q. Sun and C. Jin, *Int. J. Biol. Macromol.*, 2019, **141**, 369–377.
44 S. Deng and Y. P. Ting, *Water Res.*, 2005, **39**, 2167–2177.
45 Y. He, S. Han, H. Lin and Y. Dong, *Water, Air, Soil Pollut.*, 2020, **231**, 137.
46 D. M. Guo, Q. D. An, Z. Y. Xiao, S. R. Zhai and D. J. Yang, *Carbohydr. Polym.*, 2018, **202**, 306–314.
47 S. Zhang, Z. Wang, H. Chen, C. Kai, M. Jiang, Q. Wang and Z. Zhou, *Appl. Surf. Sci.*, 2018, **440**, 1277–1285.